JOURNAL OF GEOPHYSICAL RESEARCH: OCEANS, VOL. 118, 3608–3621, doi:10.1002/jgrc.20242, 2013

On the factors influencing the development of sporadic upwelling in the Leeuwin Current system

Vincent Rossi,[1] Ming Feng,[2] Charitha Pattiaratchi,[3] Moninya Roughan,[1] and Anya M. Waite[3]

Received 28 November 2012; revised 16 April 2013; accepted 15 May 2013; published 23 July 2013.

[1] While there is no persistent upwelling along the West-Australian (WA) coastline, sporadic upwelling events have been documented primarily in summer. By analyzing comparatively the variability of both Ekman and geostrophic cross-shore transports over a seasonal cycle, we show that the situation is more contrasted. Based on a composite index computed from satellite data over a 15 year period, calibrated with well documented events, we investigate the factors influencing the development of sporadic upwelling in the region. Overall, the occurrence of transient upwelling events lasting 3–10 days varies largely in space and time. Shelf regions at 31.5 and 34°S are favored with up to 12 upwelling days per month during the austral spring/summer. Although being generally favored from September to April, sporadic upwelling events can also occur at any time of the year at certain locations north of 30°S. On average over 1995–2010, the Ningaloo region (22.5°S) cumulates the highest number of upwelling (∼140 days per year) and is characterized by longer events. The intensity of intermittent upwelling is influenced by the upwelling-favorable winds, the characteristics of the Leeuwin Current (e.g., onshore geostrophic flow, mesoscale eddies and meanders, stratification and nitracline) and the local topography. This suggests that short-living nutrient enrichment of variable magnitude may occur at any time of the year at many locations along the WA coast.

Citation: Rossi, V., M. Feng, C. Pattiaratchi, M. Roughan, and A. M. Waite (2013), On the factors influencing the development of sporadic upwelling in the Leeuwin Current system, *J. Geophys. Res. Oceans*, *118*, 3608–3621, doi:10.1002/jgrc.20242.

1. Introduction

[2] Oceanic primary production is essentially limited by the availability of dissolved macronutrients in the usually depleted surface layers. Vertical movements bringing deep rich-nutrient waters to the euphotic zone, such as upwelling, are, therefore, of tremendous importance as they provide an essential nutritional input enhancing primary production, which eventually benefits the whole oceanic food web [*Pauly and Christensen*, 1995]. In the world ocean, one can distinguish (quasi) permanent upwelling systems driven by persistent winds (the four eastern-boundary upwelling systems and the equatorial upwelling), whereas other upwelling processes can be referred to as sporadic coastal upwelling, being restricted in space and time. Assessing the upwelling activity over continental margins has been the subject of numerous studies mainly focussed on the permanent eastern-boundary upwelling systems [e.g., *Bakun*, 1990; *Nykjaer and Van Camp*, 1994; *Alvarez et al.*, 2008]. This paper aims at studying the variable occurrence of sporadic upwelling events over the entire WA continental shelf.

[3] Surface circulation off the WA coast is dominated by the Leeuwin Current (LC) system that consists of a near-surface flow, the southward LC, the deeper northward flow of the Leeuwin Undercurrent, and transient coastal countercurrents [*Cresswell and Golding*, 1980; *Thompson*, 1987; *Woo et al.*, 2008; *Pattiaratchi and Woo*, 2009] (see also Figure 1). The LC forms off the Gascoyne shelf (20–23°S) and then consists of a relatively narrow, shallow (upper 250 m) but intense poleward warm current [*Thompson*, 1987, *Smith et al.*, 1991; *Feng et al.*, 2003]. With its core usually located between the shelf break and about 100 km offshore, it flows along the WA coast until Cape Leeuwin (35°S) and eventually extending eastward along the southern Australian coastline in winter [*Ridgway and Condie*, 2004]. In addition, due to a complex topography associated with current/frontal instabilities, meanders, and eddies spin up everywhere along the WA coast all year long, intensified during the autumn/winter period [*Rennie et al.*, 2007; *Meuleners et al.*, 2007]. The absence of large-scale upwelling and equatorward flow in the atypical LC system, as is the case in other eastern-boundary currents, has been attributed to the presence of a strong anomalous pressure gradient that drives the LC [*Cresswell and Golding*, 1980;

[1]The University of New South Wales, School of Mathematics and Statistics, Sydney, New South Wales, Australia.
[2]CSIRO Marine and Atmospheric Research, Floreat, Western Australia, Australia.
[3]The University of Western Australia, School of Environmental Systems Engineering and The Oceans Institute, Crawley, Western Australia, Australia.

Corresponding author: V. Rossi, IFISC (Institute for Cross-Disciplinary Physics and Complex Systems), UIB-CSIC, E-07122 Palma de Mallorca, Spain. (vincent@ifisc.uib-csic.es; vincent.rossi.ocean@gmail.com)

2169-9275/13/10.1002/jgrc.20242

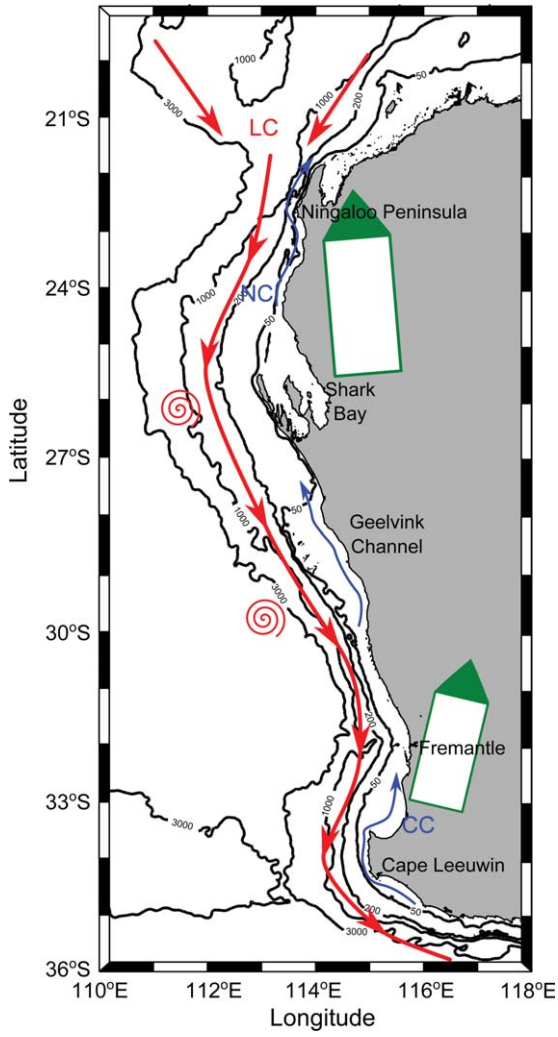

Figure 1. Map of the study area, the WA region. Thin black contours represent the bathymetry (isobaths 50, 200, 1000, and 3000 m). Note the variable width of the shelf (0–200 m). The colored annotations show the main feature of the surface circulation in the region: Red arrows are for the Leeuwin Current (LC), blue arrows are for the coastal countercurrent (Ningaloo Current, NC and Capes Current, CC), red schematic vortex represent the areas favoring mesoscale eddies formation, and green arrows are for the mean surface winds (averaged SSW within a 2° coastal band from 21° to 28°S and from 28° to 35°S, see also section 3.1).

Thompson, 1987; *Weaver and Middleton*, 1989]. This alongshore pressure gradient is set up by the Indonesian throughflow delivering warm/less saline waters from the Pacific to the Indian Ocean and by the strong surface heat loss at higher latitudes [*Smith et al*., 1991]. Despite the seasonal variation of the LC poleward transport (between ~1 and 6 Sv at 32°S), reaching its maximum during the austral autumn-winter (May-July) [*Feng et al*., 2003], the seasonal variability of the alongshore pressure gradient is unknown and is often assumed constant [*Smith et al*., 1991].

[4] Although persistent upwelling does not occur in the LC system, sporadic and localized wind-driven upwelling events have been documented primarily during the austral summer (December-March), coinciding with the minimum transport of the LC and the prominence of the upwelling-favorable (northward) winds [*Thompson*, 1987; *Weaver and Middleton*, 1989]. They have been associated with the system of equatorward coastal countercurrents inshore of the LC, the Capes Current (CC) extending along the south WA coast [*Pearce and Pattiaratchi*, 1999; *Gersbach et al*., 1999], whereas the Ningaloo Current (NC) flows intermittently along the northwest coast [*Taylor and Pearce*, 1999; *Hanson et al*., 2005; *Woo et al*., 2008]. The combination of these intermittent wind-driven coastal currents and upwelling during summer drives with localized enrichment of the usually nitrate-depleted surface waters [*Lourey et al*., 2006], enhancing primary production [*Hanson et al*., 2005; *Hanson and McKinnon*, 2009]. Clearly, the study of intermittent/localized upwelling in this oligotrophic region becomes critical to understand the links between boundary current physics and biological productivity. These sporadic upwelling events have been observed along the WA coast from the southwest region [*Gersbach et al*., 1999] to the Gascoyne shelf [*Hanson et al*., 2005; *Woo et al*., 2006].

[5] However, their transient character, their moderate intensity (leading often to subsurface expression only), and the presence of the LC itself offshore prevent the effective use of satellite sea-surface temperature (SST) as an upwelling proxy [*Pearce and Pattiaratchi*, 1999; *Furnas*, 2007]. Moreover, even when coastal SST measurements vary as a result of upwelling intensity, SST itself only indirectly reflects this intensity since strong wind, for example, results in mixing of upwelled waters and warmer surrounding waters at the sea surface. As such, previous work concentrated on developing analytical models to predict the occurrence of upwelling on this unique coast. *Thompson* [1987] proposed a simple analytical model considering the balance of forces between the alongshore steric pressure gradient, the wind and bottom stress in the alongshore direction, suggesting the existence of a specific isobath acting as the cross-shore limit of the circulation driven by the wind (inner shelf) and of the circulation driven by the large-scale pressure gradient (outer shelf). *Gersbach et al*. [1999] extended this approach to investigate the Ekman transport and its impacts on the local inner shelf flushing rates off south WA coast, predicting that upwelling occurs when the transition depth is at the 50 m isobath for a threshold period, occurring 5–9 times in summer. The local nature of this study and its simple parameterization (e.g., constant pressure gradient and simple shelf topography) limits its use along the entire WA coast. Recently, moored time series off the Ningaloo region studied by *Lowe et al*. [2012] revealed that there is in fact no consistent summer wind-driven countercurrent (NC) and that upwelling was not limited to summer periods. Another new study documented unambiguous observational evidence of an intermittent upwelling event occurring in autumn [*Rossi et al*., 2013]. To our knowledge, the probability of occurrence of these sporadic wind-driven events, their spatiotemporal variability, frequency and duration, remain largely unknown along the WA coast.

[6] Using satellite and climatological data sets, this paper investigates the seasonal variations of the main drivers of upwelling over the WA shelf, namely the alongshore

wind stress and pressure gradient. Based on a composite upwelling index, which takes into account both local and synoptic factors in a realistic setting adapted to the LC system, we then examine the spatiotemporal variability of these intermittent processes. In addition, we use previously published evidence of upwelling events to calibrate our upwelling index and to study the probability of occurrence of sporadic upwelling events along the entire WA coast. Finally, we discuss the formulation of the index, the impact of each factor taken independently and the far-reaching implications of our results.

2. Data and Methods

2.1. Remotely Sensed Data

[7] Multiple years long archives of remote sensing products, including sea-surface height (SSH) and sea-surface wind (SSW), covering the whole WA coast, are used to analyze the factors influencing the development of upwelling, namely the alongshore wind stress and the cross-shore geostrophic velocities.

[8] We used a composite SSW gridded product which consists of high-resolution ocean surface vector winds and wind stresses on a global 0.25° grid, at a daily temporal resolution from 1995 to 2010. The wind speeds were generated by blending observations from multiple satellites (up to six satellites since June 2002), while the wind directions came from the NCEP Reanalysis 2 and were interpolated onto the blended speed grids. The blending of multiple-satellite observations fills in the data gaps (in both time and space) of the individual satellite measurements reducing aliasing and random errors [*Zhang et al*., 2006]. As some near-coastal regions exhibited contamination due to the interpolation scheme, spurious values have been disregarded from our analysis (see also www.ncdc.noaa.gov/oa/rsad/air-sea/seawinds.html).

[9] We also compare the previous blended product to the wind field derived from the widely used QuikSCAT scatterometer (daily product at 0.25° resolution, covering only the period 1999–2009).

[10] We selected an SSH field calculated from mapped altimetric sea level anomalies combined with a mean dynamic topography to derive the geostrophic surface currents. The mapped sea level anomaly merging measurements from several altimeter missions are combined with the mean dynamic topography (due to the permanent ocean circulation, with the marine geoid removed) of *Rio et al*. [2009] to obtain a time-variable SSH product. To match the other satellite products, the original weekly SSH data on a 1/3° Mercator grid were converted to daily data onto a 0.25° regular grid using a standard bilinear interpolation algorithm. More details on the computation of the geostrophic velocities are given by *Sudre et al*. [2013].

2.2. Climatological Data Sets

[11] The surface zonal transport due to the alongshore pressure gradient which drives the LC can also be assessed by vertical integration of the thermal wind law using the density gradient derived from climatological data sets. Climatological density fields along the WA shelf are extracted from the objectively analyzed fields of temperature [*Locarnini et al*., 2010] and salinity [*Antonov et al*., 2010] from the World Ocean Atlas 2009 (WOA09) as well as from the Climatological Atlas of Regional Seas (CARS09) [*Condie and Dunn*, 2006]. Note that these gridded data sets have different resolution: CARS09 has a $1/2^\circ$ spatial horizontal resolution, up to 79 vertical levels and a daily temporal resolution, whereas WOA09 has a 1° spatial horizontal resolution, only 24 vertical levels and a monthly temporal resolution.

[12] From these climatological data sets, different methods can be applied to estimate the zonal velocities. On one hand, the upward integration of the thermal wind law requires the definition of the surface layer of interest, the top 100 m (∼mean depth of the mixed layer depth (MLD)) and of a deep reference level, 1000 m, where no motion is assumed [*Woo et al*., 2008]. The cross-shore geostrophic velocities can then be computed locally from the alongshore geopotential anomaly along the 1000 m isobaths, using a 1° (2°, respectively) moving window based on CARS09 (WOA09, respectively), resulting in a final resolution of $1/2^\circ$ (1°, respectively). However, zonal velocities calculated this way (not shown) do not necessarily represent the surface dynamics well as they integrate hydrological information (alongshore density gradient) from much deeper water. Moreover, because the "no motion" assumption might not be true and since such climatological data set usually lacks accuracy/resolution in the deep ocean, this calculation was not retained. On the other hand, to reconcile geostrophy at the surface and thermal wind law within the water column, one can apply a downward integration of the thermal wind law from the surface to the depth of interest (∼100 m) in addition of the SSH gradient (surface slope) to infer the total zonal geostrophic velocities within the surface layer.

2.3. A Composite Upwelling Index

[13] To investigate sporadic upwelling over the WA coast, we used an approach developed by *Marchesiello and Estrade* [2010] who derived an improved dynamical upwelling index that accounts for the role of alongshore pressure gradients counteracting the coastal Ekman divergence within a realistic innershelf configuration. Their novel analytical model is particularly well adapted for the WA region since it takes into account the effect of onshore geostrophic flow on the structure of upwelling, thus adding crucial information to the classical wind-based upwelling index [e.g., *Bakun*, 1990; *Alvarez et al*., 2008]. The Ekman upwelling index (EUI, related to Ekman "divergence") and the geostrophic upwelling index (GUI, due to the coastal geostrophic "convergence") combine to form the composite upwelling index (CUI):

$$\mathrm{CUI} \approx \mathrm{EUI} + \mathrm{GUI} \approx \frac{\tau_A}{\rho f L_U} + \frac{u_G D}{2 L_U} \qquad (1)$$

where τ_A is the alongshore wind stress (positive when upwelling favorable, that is, alongshore equatorward), u_G is the geostrophic cross-shore velocity (positive offshore), ρ is the water density, and f is the coriolis parameter. L_U is a scaling factor calculated as the larger of the ratio of the vertical Ekman layer scaled by shelf topography and the horizontal Ekman layer L_E:

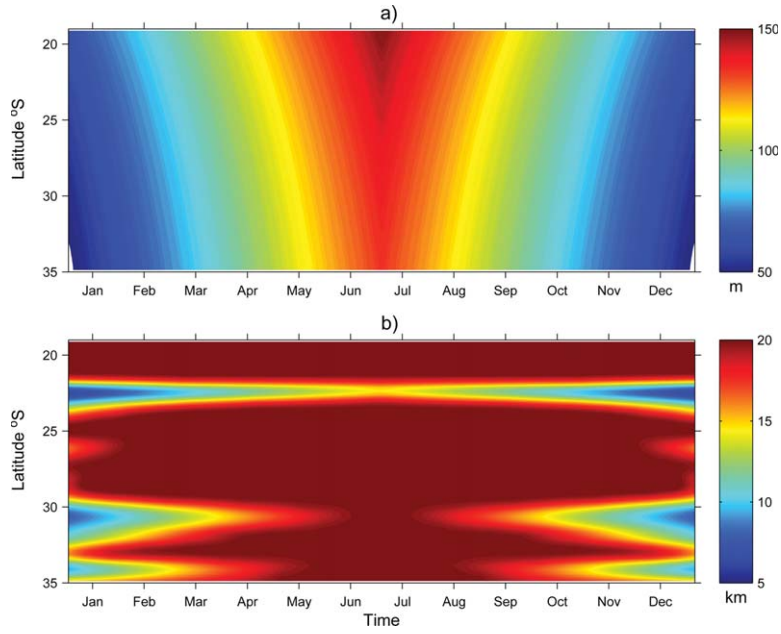

Figure 2. Parameters used in the computation of the composite upwelling index [*Marchesiello and Estrade*, 2010] as a function of latitude and time (*x*-ticks indicate the 15th of each month). Consistent with our climatological approach, (a) the depth of the Ekman layer $D(y,t)$ and (b) the topographical scaling factor $L_U(y,t)$ are varying with latitude y and time t.

$$L_U = \max\left[\frac{0.75D}{S};\ L_E = \pi\ \sqrt{2A_H/|f|}\right] \tag{2}$$

where D is the vertical Ekman layer, considered equivalent to the MLD in this work, calculated as

$$D = \pi\ \sqrt{2A_V/|f|} \tag{3}$$

[14] S is the shelf slope (ratio of the maximum depth versus the shelf width, oscillating between 10^{-3} and 10^{-2}). As prescribed by *Marchesiello and Estrade* [2010], a maximum value of 20 km is imposed for L_U to avoid counting double-cell structures for extended shelves. A_V is the vertical viscosity ($A_V \sim 0.01$ m^2 s^{-1}) and A_H is the horizontal viscosity ($A_H \sim 100$ m^2 s^{-1}), chosen following *Marchesiello and Estrade* [2010]. Our results are insensitive to the slight latitudinal changes of density within surface waters and we have thus retained a constant density of $\rho = 1023$ kg m^{-3}.

[15] All indexes EUI, GUI, and CUI are in m/day and represent the theoretical vertical velocities due to: The Ekman divergence, the coastal geostrophic convergence, and their combination, respectively. The main direction of the coastline along the WA coast is particularly variable; hence, we compute the indexes in the shore-normal, rather than zonal, direction to optimize our interpretations. To do this, it requires localizing the coastline and estimating its orientation on a scale consistent with the forcing parameters (~25 km, i.e., 1/4°). The isobath 50 m is used in order to "close" the large embayment such as Shark Bay and to take into account the extended shallow lagoons observed at some locations along the WA coast (e.g., Abrolhos Islands). A smoothing procedure is then applied to the high resolution (1 arc min) topographic data set to remove small-scale variability of the coastline. All forcing parameters (wind, bathymetry, and currents) were thus projected along the main coastline orientation and only the cross-shore and alongshore projections (rotated appropriately) were used for further calculations.

[16] This analytical model includes simple parameterizations of the upper layers stratification and of the shelf topography. According to the initial version developed by *Marchesiello and Estrade* [2010], the Ekman layer depth $D \approx$ MLD depends only on the Coriolis parameter. However, to be consistent with our climatological approach, we must add a temporal variation to represent the intraannual variability of the MLD. We used the values reported by *Rousseaux et al*. [2012] and *Lowe et al*. [2012] who studied the seasonal cycle of the MLD over the Ningaloo region using complementary in situ observations (a near-shore mooring and multiple field surveys) and a numerical model. In particular, both studies agreed on the shallower MLD of ~40–60 m observed in December/January/February and the deeper ones of about ~150 m in May/June/July. Following equation (3) with a constant $A_V = 0.01$ m^2 s^{-1}, an estimate of $D \approx$ MLD which includes a latitudinal variation due to f is calculated (not shown). We retained this latitudinal profile (using $A_{\text{V-summer}} = 0.01$ m^2 s^{-1}) for 1 January as it leads to MLD ~60 m at 22°S, corresponding to a typical summer situation in the region. Expressing A_V as a function of D (equation (3)), we impose the winter MLD $\approx D =$ 150 m at 22°S and we derive a new $A_{\text{V-winter}} \approx 0.06$ m^2 s^{-1}. This parameter is then used to compute a winter profile (retained for 1 July) varying with latitude (equation (3)). The seasonal modulation of $D \approx$ MLD is finally obtained by a bilinear spatiotemporal interpolation of these profiles (Figure 2a). Note that the resulting values of $A_V \in [0.007\ ;\ 0.06]$, D varying from 50 to

150 m, are consistent with the theoretical value prescribed by *Marchesiello and Estrade* [2010], the winter periods being associated with higher vertical eddy viscosity. There are important seasonal variations of $D \approx$ MLD, considerably deepening in autumn/winter, as compared to summer periods.

[17] The continental shelf width (defined from 0 to 200 m isobaths) and its slope change remarkably along the WA coast (see Figure 1). The continental shelf is very wide (>150 km) north of 21.5°S and then extremely narrow (∼20 km) off the Exmouth peninsula (22.5°S). South of Point Cloates, it widens gradually with a 40 km wide shelf at 23°S, increasing to 85–100 km around Shark Bay (25–28°S). Note that the orientation of the coastline changes sharply at 25.5°S. To the south of Shark Bay, the continental shelf width decreases to reach a local minimum of ∼40 km at 31°S, and then widens again offshore Fremantle and Bunbury (∼60–80 km at 32–33°S). A noticeable narrow shelf of ∼45 km is present at 34°S, between Cape Naturaliste and Cape Leeuwin. To take into account, the influence of the changing width of the continental shelf on the upwelling process, a parameterization L_U is included in the analytical model following equation (2). When deep winter MLD increases the term $\frac{0.75D}{S}$, L_U becomes essentially limited by the imposed value of 20 km since very large shelves are not found in this area. The shallow MLD in summer decreases the term $\frac{0.75D}{S}$ which may reach values lower than L_E (itself ranging from 4.5 to 6.5 km over WA coast). In particular, $L_U = L_E$ only at the narrow shelf of Ningaloo during summer and $L_U = \min\left[\frac{0.75D}{S},\ 20\ \ \text{km}\right]$ otherwise because of the maximum value imposed by *Marchesiello and Estrade* [2010]. Note that the effect of the narrow continental shelves at 22.5°S, 31°S, and 34°S appears to be maximal in summer when the MLD is relatively shallow (Figure 2b).

[18] *Marchesiello and Estrade* [2010] derived and validated the index against the solution of a primitive equation model from the New-Caledonia region, that is, at similar latitudes as this study. Additionally, focussing on the world's four largest eastern-boundary upwelling regions, their composite index presented a better fit to an independent upwelling index based on SST, as compared to the classical wind-based Bakun's index [*Bakun*, 1990].

2.4. Climatological Analysis

[19] To compute the CUI in a cross-shore direction, we used high resolution satellite products of SSH and SSW to compute the GUI and EUI, respectively. More specifically, the projected alongshore wind stress (upwelling favorable, parallel to the coastline and positive equatorward) is computed from the SSW and is then combined with the scaling factors to derive the EUI. From the SSH field, the geostrophic currents are computed as given by *Sudre et al*. [2013] and the projected cross-shore geostrophic velocities (positive offshore) are extracted to derive the GUI in association with the scaling factors described previously. The composite index CUI (positive in the offshore direction) is finally calculated as the sum of the two former components (equation (1)). To better understand the physical interactions, the variability of both Ekman divergence and geostrophic convergence are first analyzed separately, and then after their combination into the CUI, in a climatological setting. A two-dimensional smoothing procedure is applied to decrease the impact of intense small-scale coastal features of moderate reliability (at the limit of validity of satellite data), without removing the mesoscale signals (such as eddies and meanders). All climatologies were built by averaging 15 years of data (1995–2010) over 5 day windows within a coastal band of 2° width (zonal extension), every 1/4° (meridional extension), in accord with the resolution of the satellite product. Several sensitivity analyses were performed using different widths for the coastal band and apart from diminishing the general amplitude, the main patterns remain relatively unchanged.

3. Results

[20] The alongshore pressure gradient driving the LC is responsible for an onshore geostrophic transport counteracting the wind-driven Ekman transport. In the following, we first analyzed both terms taken independently, namely the offshore Ekman transport (section 3.1) and the onshore geostrophic surface velocities (section 3.2). Then, we use the analytical model of *Marchesiello and Estrade* [2010] to examine the main factors involved in the upwelling process in this region (section 3.3). Finally, we used well-documented event to calibrate our indexes and to study the occurrence of sporadic upwelling events over the WA coast (section 3.4).

3.1. Variability of the Upwelling-Favorable Winds

[21] Following *Alvarez et al*. [2008], we analyzed the theoretical offshore Ekman transport perpendicular to the coastline $Q_\perp$ (positive offshore) as the main variable for wind-driven upwelling by means of:

$$Q_\perp = \cos(\alpha)Q_x - \sin(\alpha)Q_y \tag{4}$$

where α is the angle between the unity vector pointing westward and the normal vector to the coastline pointing offshore (positive in a clockwise direction), (Q_x, Q_y) being the zonal and meridional component of the Ekman transport.

[22] Different latitudinal regimes of upwelling favorable winds are observed along the WA coast (Figure 3). Although it shows a maximum (1500–2500 $m^3\ s^{-1}\ km^{-1}$) during the austral spring/summer (August–April), the winds are upwelling favorable all year long from 21.5° to 26.5°S with moderate offshore Ekman transport during winter (500–1000 $m^3\ s^{-1}\ km^{-1}$). Further south from 26.5° to 31°S, the wind stress is upwelling favorable during spring/summer with similar offshore Ekman transport to the northern area (1500–2500 $m^3\ s^{-1}\ km^{-1}$). However, it is very weak or slightly negative (−500 to 500 $m^3\ s^{-1}\ km^{-1}$) from May to September. South of 31°S, there is upwelling favorable Ekman transport (1000–2000 $m^3\ s^{-1}\ km^{-1}$) from late October to March, whereas it is negative (−1500 to −500 $m^3\ s^{-1}\ km^{-1}$), corresponding to onshore transport and downwelling from April to September. A particular pattern is observed at 33–34°S, where a weak positive Ekman transport (0–500 $m^3\ s^{-1}\ km^{-1}$) prevails during winter months due to the meridional coastline. Note that north of 21.5°S, the signal is weak or negative all year long due to the sharp change in the coast orientation.

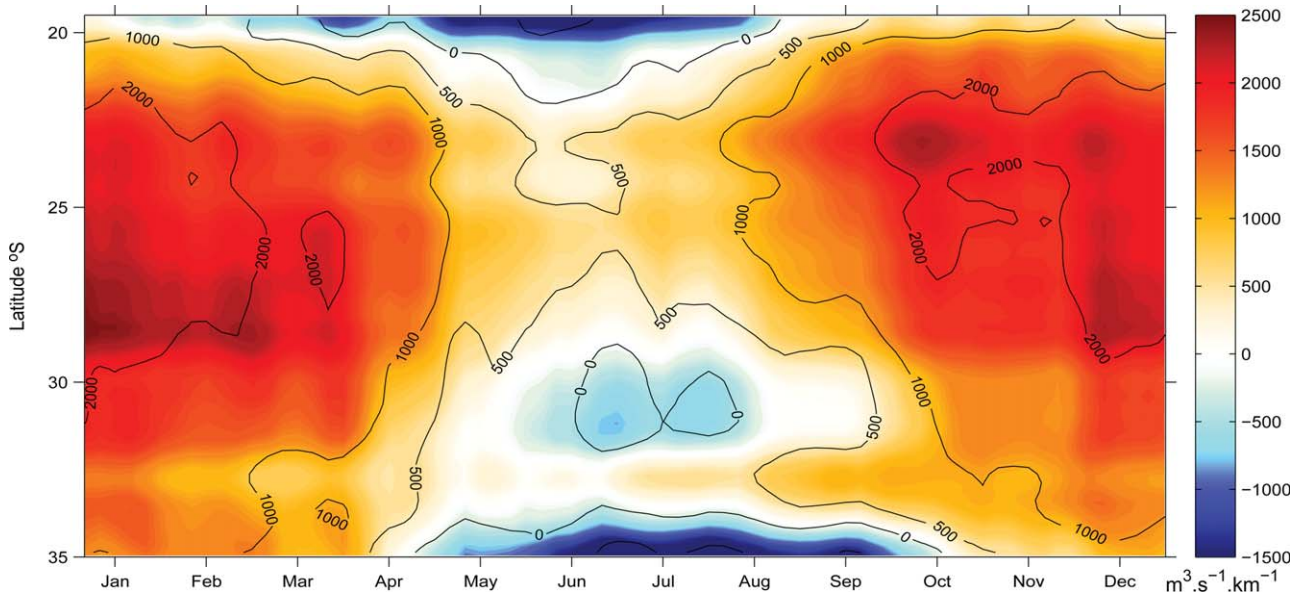

Figure 3. Hovmöller diagram (latitude versus time) of the theoretical offshore Ekman transport $Q_{\perp}$ (in $m^3\ s^{-1}\ km^{-1}$ of coastline) based on the blended SSW product (1995–2010). Black contours represent the same variable computed from the QuikSCAT archive (1999–2009).

[23] Overall, the southern regions are affected by slightly different wind regimes than the northern areas. In average, coastal winds of 7.2 m s^{-1} directed to the north/northeast (wind vector azimuth +15°, with respect to true north) occur in the southern regions (28–35°S), while the northern ones (21–28°S) see winds of 8.3 m s^{-1} blowing to the north/northwest (wind vector azimuth −5°; see also the annotations in Figure 1). The northern areas are thus most consistently forced by upwelling favorable winds, while the varying coastline orientation explains most of the smaller scale variability of the offshore Ekman transport.

[24] These general wind patterns and their amplitude are very consistent in both wind products (see black contours in Figure 3), thus strengthening our results. These products have been validated for both open and coastal ocean application [*Pickett et al*., 2003; *Zhang et al*., 2006]. In addition, a good consistency is found between the theoretical offshore Ekman transport computed from the blended product and from the wind data simultaneously collected during a field survey off Ningaloo Peninsula [*Rossi et al*., 2013] (not shown). Due to its extended temporal coverage (1995–2010), the blended product was retained for the computation of the indexes.

3.2. Seasonal Variation of the Geostrophic Flow

[25] We now analyzed the zonal geostrophic velocities u_G acting as a limiting factor for upwelling along the WA coast. Although *Smith et al*. [1991] suggested that the large-scale alongshore geopotential gradient driving the LC is almost constant all year long, there is growing evidence that it is not the case [*Godfrey and Ridgway*, 1985], especially at smaller scales [*Lowe et al*., 2012].

[26] Estimates of the zonal geostrophic velocities (positive westward) computed from the SSH archive alone and from its combination with climatological data sets (WOA09 and CARS09) are comparatively analyzed (Figure 4). Overall, the different estimates of u_G, all representative of the flow in the surface mixed layer (∼100 m), are in relatively good agreement with similar amplitudes (±0.05 m/s). The main patterns obtained from the remote sensing analysis (Figure 4a) are essentially conserved when combined with the climatological data sets (Figures 4b and 4c) as the SSH dominates the signal. Note, however, that the onshore (negative) velocities are attenuated, while the patchy offshore (positive) velocities are slightly reinforced. This seems due to the subsurface density field (positive poleward, see also *Woo et al*. [2008]) that tends to counteract the strong geostrophic convergence at the surface. The zonal geostrophic velocities are generally onshore (negative values), with an intensification (up to −0.1 m/s) during the autumn/winter months. This intensification occurs primarily in the northern regions (at 21–24°S from April to July) and propagates further south slightly later (at 31–34°S from June to September). The intense permanent onshore flow observed consistently at 26.5°S seems to be a robust feature of the area. The presence of offshore geostrophic flow is also observed similarly in all three computations. Although both their occurrence and amplitude are slightly variable between the different data sets, they are found at similar latitudes (22.5°, 25.5°, 28°, and 34°S) essentially from March to August (autumn/winter).

[27] Still, some discrepancies exist such as the magnitude of the offshore flows. These discrepancies, potentially impacting the computation of the GUI (and thus of the CUI), can be attributed to different factors: (i) hydrography climatologies may be affected by interpolation scheme close to the shelf topography, (ii) mesoscale meanders/eddies are resolved by the satellite but less likely by WOA09/CARS09, (iii) CARS09, WOA09, and the satellite SSH have different spatial and temporal resolution, and (iv) interannual/interdecadal variability is important in this

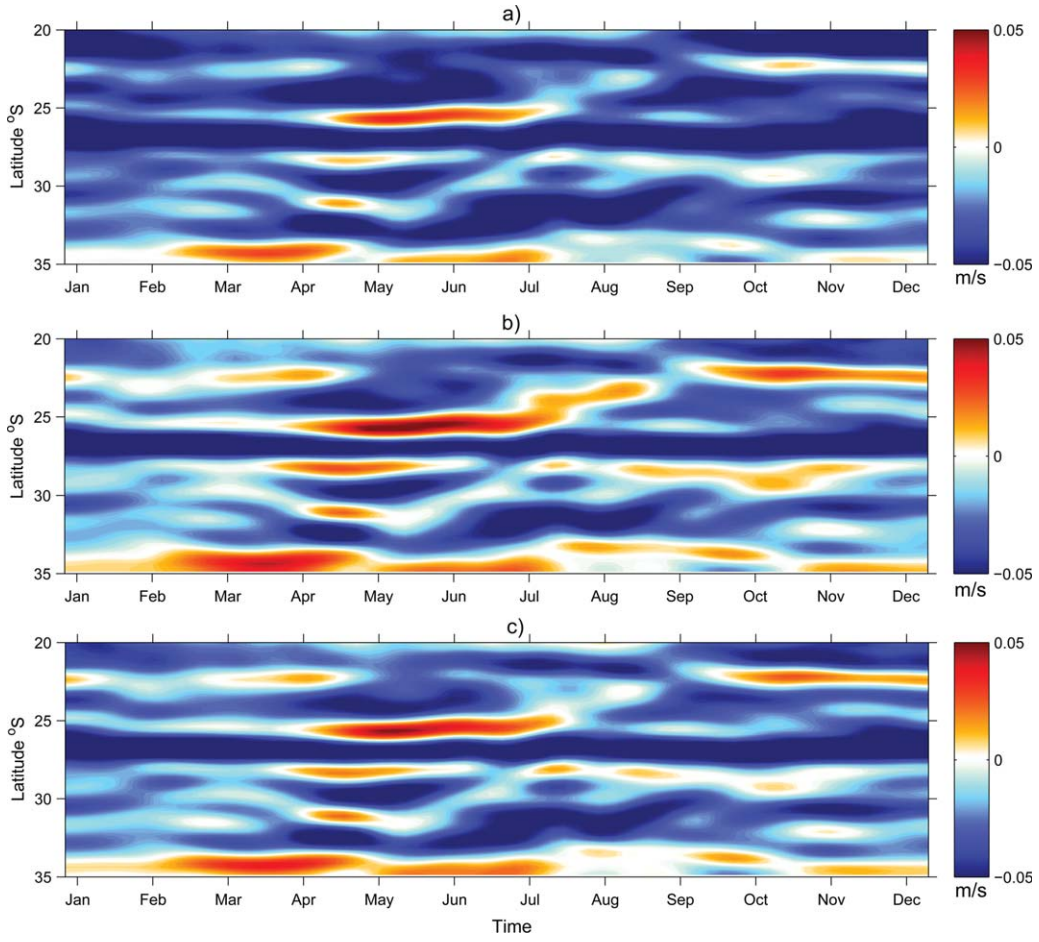

Figure 4. Hovmöller diagrams (latitude versus time) of the surface geostrophic cross-shore velocities u_G (positive values correspond to an offshore/westward current). Climatology of u_G as deduced (a) from the whole SSH archive (1995-2010) alone and from its combination with a downward integration (0-100 m) of the thermal wind law based (b) on CARS09 and (c) on WOA09 (see also section 2.2).

system [*Feng et al*., 2008, 2013] and so is the temporal period used to build the climatology.

[28] To reduce the uncertainties inherent to the CUI formulation and to the data sets used for its computation, we used only satellite data sets with u_G derived from SSH and τ_A calculated from the blended SSW. For consistency, EUI and GUI are computed on similar remote-sensed archives with the same temporal/spatial resolution (resolving mesoscale meandering and eddies of the LC), which can be easily projected against the orientation of the coastline (both zonal and meridional components being available) and having the same temporal coverage (1995–2010).

3.3. Spatiotemporal Variability of Sporadic Upwelling Over the West-Australian Coast

3.3.1. Climatological *A*nalysis of the *M*ean EUI

[29] The analysis of the EUI, calculated as the offshore Ekman transport divided by the scaling factor L_U (Figure 5a), reflects that of the offshore Ekman transport alone (section 3.1). However, the overall effect of the division by L_U is a decrease in strength of the wind-driven upwelling in winter due to the thicker MLD, and the indirect effect of the narrow shelves (in particular at 22.5° and 31°S) that strengthen the latitudinal variation of the offshore wind-driven Ekman transport, resulting in three latitudinal maxima in EUI (22.5°, 31°, and 34°S).

3.3.2. Climatological *A*nalysis of the *M*ean GUI

[30] Following equation (1), the horizontal cross-shore geostrophic velocities u_G (derived from SSH) are combined with previously described scaling factors to obtain the GUI (Figure 5b). As predicted by the theory, a negative (positive) GUI corresponds to an onshore (offshore) geostrophic flow, associated to downward (upward) theoretical vertical velocities, thus driving downwelling (upwelling) process [*Marchesiello and Estrade*, 2010]. The GUI is mainly negative everywhere due to the onshore geostrophic flow driven by the large-scale alongshore pressure gradient responsible for the downwelling signal commonly observed in the LC system [*Woo et al*., 2008; *Pattiaratchi and Woo*, 2009; *Rossi et al*., 2013]. However, some spatiotemporal variations of the geostrophic limitation are observed along the WA coastline. The GUI is clearly negative from April to September, which is consistent with the period of maximum transport in the LC [*Feng et al*., 2003]. For the rest of the year (September to the end of March), the GUI is less

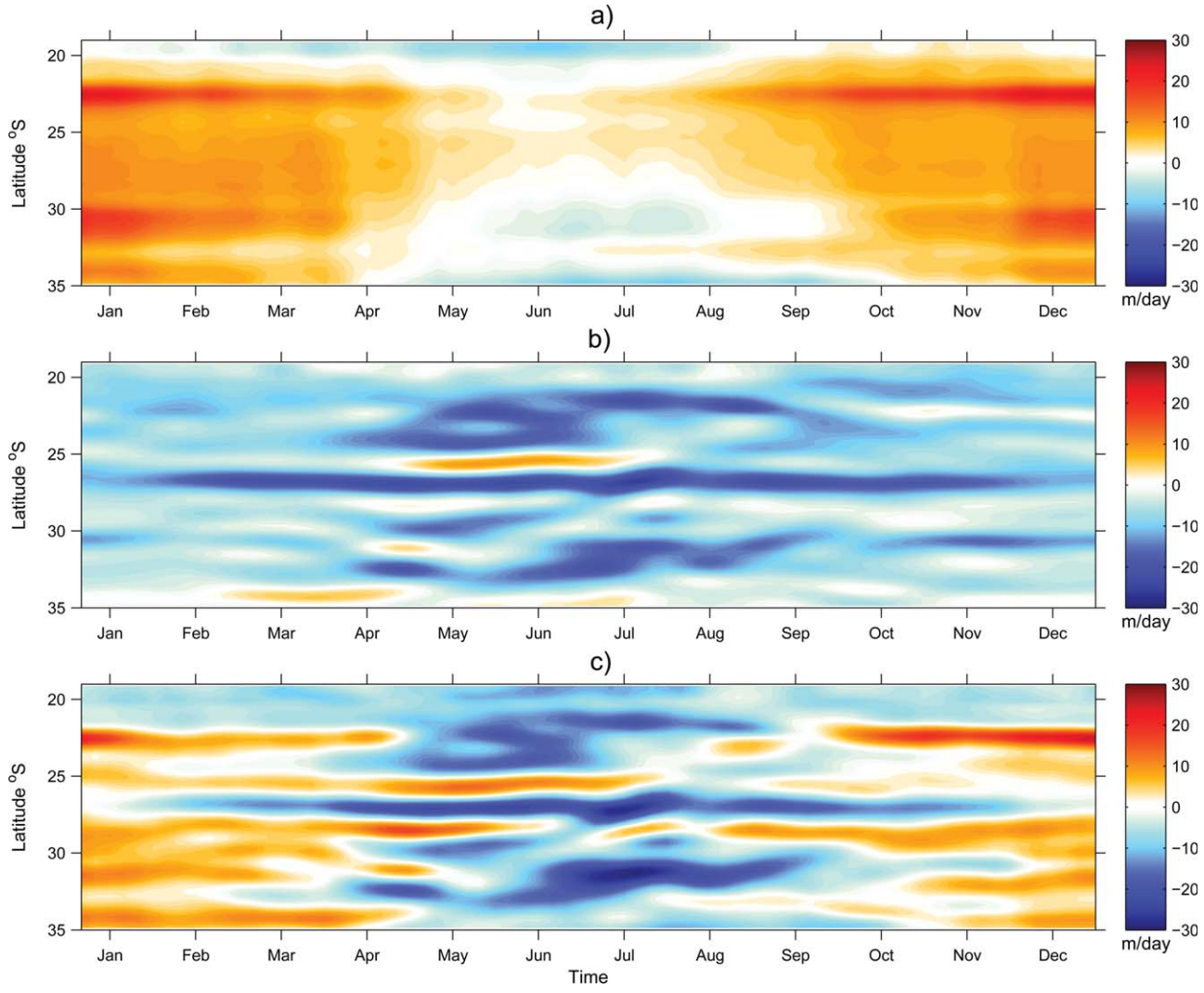

Figure 5. Hovmöller diagrams (latitude versus time) of (a) the Ekman upwelling index (m/day, equivalent to vertical velocities), (b) the geostrophic upwelling index (m/day, equivalent to vertical velocities), and (c) composite upwelling index (in m/day of vertical velocities, a combination of the two previous components). Red colors represent a balance of forces favoring upwelling events.

intense, partly due to a shallow MLD and weaker LC (itself influenced by the variable alongshore pressure gradient and the opposing winds). There are also some specific periods/locations, where the geostrophic limitation is particularly strong: Negative GUI (i.e., downwelling) is found during the late autumn period (May–July) between 21° and 24°S and slightly later (June–September) further south around 31–34°S (Figure 5b). At about 26.5°S, there is a band of strongly negative GUI almost all year long, diminishing only for December/January. In contrast, at 25.5°S (April-July), at 28.5°S (April-November), and at 34°S (February-April) the GUI is null or even positive, resulting in no limitation or even offshore geostrophic transport, thus strengthening the wind-driven upwelling.

3.3.3. Climatological *A*nalysis of the *M*ean CUI

[31] By summing up the individual components EUI + GUI = CUI (Figure 5c), we can examine together the combined variability of Ekman and geostrophic forcing. Overall, the CUI ranges from ±30 m/day in our climatology and decreases down to ±10 m/day when annually averaged. The extreme and mean values for the Leeuwin system are lower but consistent with the annual means presented in the four major upwelling systems where strong persistent upwelling occurs, reaching up to 25 m/day (Table 1). The negative average CUI (−2.3 m/day) and the complex patterns observed in the climatology confirm that upwelling is not a persistent feature but shows strong seasonality over the WA coast. In general, our results show that the upwelling season along the WA coast is slightly longer than previously thought, going from mid-August to mid-April along almost the whole west coast. After the winter relaxation period, the upwelling favorable season starts earlier in the north, beginning from early August onward, whereas it starts only from mid-September in the south. The southern regions (30–35°S) appear almost equally favored but only during the upwelling season, whereas the situation is more contrasted in the north. Upwelling is favored all year long at

Table 1. Comparison of Annually Averaged CUI Between the World's Eastern Boundary Current Systems (as Given by *Marchesiello and Estrade* [2010])

Mean CUI (m/day)	Leeuwin (20–35°S)	Humboldt (10–40°S)	Benguela (15–35°S)	Canary (20–40°N)	California (25–45°N)
Minimum	**−15**	1	2	1	2
Average	**−2.3**	8.5	12	8	7
Maximum	**9**	17	25	18	20

some locations, probably due to the stronger alongshore wind stress than in the south, while there are other areas in which upwelling inhibited. There are indeed latitudinal bands, where the balance is particularly favorable for the development of upwelling: 22–23°S (Ningaloo reef)/25.5°S/28.5°S (Gelvink channel)/31.5°S and 34°S (CC). Surprisingly, there is a marked positive index from April to August at 25.5°S and 28.5°S during the wind relaxation period, probably due to the offshore geostrophic component at this temporal/latitudinal window. On the contrary, a negative balance favoring downwelling is observed all year long south of Shark Bay (26.5°S), mainly due to the strong geostrophic limitation.

3.4. Occurrence of Sporadic Upwelling Events Over the West-Australian Coast

[32] Based on this climatological analysis, and in accord with previous studies [e.g., *Pattiaratchi and Woo*, 2009], sporadic upwelling should not be favored during autumn/early winter in the Ningaloo Peninsula region. However, the climatology of CUI is potentially underestimating the occurrence of these processes due to their highly sporadic nature. Indeed, the averaging procedure to obtain our climatological indexes results in subsequent smoothing of their magnitude due to highly variable (positive and negative) values. This is the reason why complementary information can be obtained through statistical analyses of upwelling events based on a threshold of CUI (rather than simple time averages).

[33] In order to test the reliability of the CUI and to define a threshold index favoring upwelling, one can record its evolution for specific upwelling events that have been previously identified and thoroughly studied. In particular, *Hanson et al*. [2005] and *Woo et al*. [2006] have documented a sporadic upwelling event based on a field survey off WA coast (including the Ningaloo Peninsula) during November 2000. In addition, *Lowe et al*. [2012] presented an outstanding remote-sensed evidence (SST, their Figure 1) of a localized upwelling along the Ningaloo Peninsula in January 2007. More recently, *Rossi et al*. [2013] clearly showed the occurrence of a localized upwelling and associated countercoastal current (NC) over the southern Ningaloo shelf in May 2010. We thus extracted the temporal evolution of a spatial mean of the CUI over the Ningaloo region during these three periods that have been previously identified as "upwelling" (Figure 6). During these specific events occurring, respectively, in late spring, early summer, and midautumn, the CUI increases from negative or weakly positive values to strongly positive (>15 m/day). In particular, concerning the event of May 2010, a clear raise of the index (reaching 15 m/day or more) is observed from the 19 May till the end of May, coinciding with the observational evidence of localized upwelling and current-reversal (NC) [*Rossi et al*., 2013]. Indeed, their observations tend to indicate that 3 days or more of upwelling favorable forcing generated coastal upwelling in this area. Based on the previous observations (Figure 6), a CUI greater than 15 m/day during at least 3 days would be associated to coastal upwelling, independently of the season concerned. Although this threshold might potentially disregard the weak upwelling, all events of less than 3 days (and/or characterized by $0 < \mathrm{CUI} < 15$) are ignored to focus only on the significant upwelling that are very likely to drive an oceanic response.

[34] Using a threshold of $\mathrm{CUI} \geq 15$ m/s for a minimum period of 3 days, we monitor the number of events matching these criteria over the last 15 years (1995–2010). The events are counted over the period 1995–2010 by averaging the CUI over an area of 2° in longitude and 0.25° in latitude along the entire WA coast. Based on a climatological analysis of 15 years of satellite data, the results show the mean numbers of upwelling favorable days per month (Figure 7a) and per year (Figure 7b).

[35] The mean number of upwelling days per month oscillates between 0 and 18 days, depending on the season and the location. The strong seasonality in the occurrence of upwelling events is evidenced by a range of 8–18 days of upwelling during the season (spring/summer, maximized at certain latitudes), whereas it never exceeds 10 days during autumn/winter, except at the most favorable location. Whilst the upwelling season in the south is confined to the spring/summer months (October to mid-March), it is generally longer further north since sporadic upwelling events still occurs during the autumn/winter months. From March to September, there are between 5 and 11 days at 22.5°S, 25.5°S, and 28.5°S, mainly due to the almost constant favorable wind stress and the weak or even reverse onshore geostrophic limitation during this period. Overall, based on the mean number of favorable days per year for upwelling, the preferential latitudinal bands for upwelling are confirmed: 22.5°S (∼140 days/year), 28.5°S (∼125 days/year), 31.5°S (∼90 days/year), and 34°S (∼70 days/year) (Figures 7a and 7b).

[36] A brief analysis of the duration of the events (not shown) reveals that about 90% of the total events monitored are comprised of 10 or less consecutive upwelling favorable days ($\mathrm{CUI} > 15$ m/day), whereas less than 10% of the events are longer than 10 days. Note there is only one location (22.5°S) where the duration of upwelling favorable forcing is significantly higher, that is, ∼20% of the events monitored are longer than 10 days. Although statistically occurring more in spring/summer, it is seen that the latitude of Ningaloo reef (22.5°S) is in fact one of the unique locations along the WA coast benefiting from upwelling events all year round (between 5 and 18 days). Another interesting observation is the presence of upwelling events during autumn/winter, between 4 and 10 days per months, south of the Ningaloo peninsula (25.5°S). The model estimates that in the Ningaloo region, an average alongshore wind speed of ∼14 m/s is required for the CUI to reach a threshold of 15 m/day in winter (June), whereas only speeds ≥9 m/s are needed in summer (December).

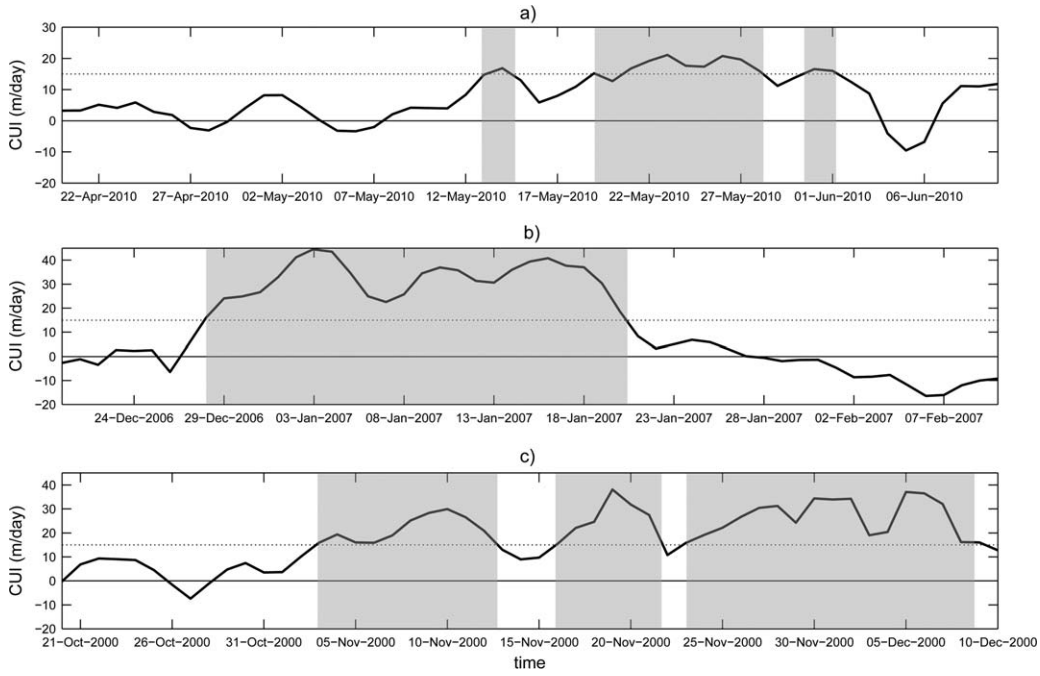

Figure 6. Calibration of the composite upwelling index. CUI (m/day) time series off Ningaloo (a) during May 2010 [*Rossi et al*., 2013], (b) from mid-December 2006 to January 2007 [*Lowe et al*., 2012], and (c) from late October to early December 2000 [*Hanson et al*., 2005; *Woo et al*., 2006]. The upwelling periods, when CUI > 15 m/day (threshold symbolized by the black dotted line) are shaded in gray.

4. Discussion

4.1. Index Formulation

[37] The occurrence of upwelling was investigated by studying simultaneously Ekman divergence and geostrophic convergence along the whole WA coast using density climatologies and remotely sensed wind and SSH data sets. Results from a recent modeling study (J. Xu, personal communication, 2012) indicated that the alongshore pressure gradient had a strong influence on the alongshore currents, but less so on the cross-shelf transport, itself well characterized by simple Ekman theory. However, it is suggested that Ekman theory could not accurately predict the structure of the cross-shore transport along this coast as it is influenced by transient mesoscale features, the stratification and the shelf topography. Our approach derived from *Marchesiello and Estrade* [2010] is indeed particularly adapted since it takes into account all the important parameters identified above, including persistent mesoscale features and their dynamical signatures. Additional effects could be included in our analytical model such as a parameterization of the undercurrent, of the wind-curl effect, of the bottom Ekman layer and the three dimensionality. Nevertheless, we believe our index is robust in the first order as it includes all the major factors operating in this region, allowing its future application to study the interannual/interdecadal variability, known to strongly impact the WA shelves [*Feng et al*., 2013].

4.2. Variability of Ekman and Geostrophic Cross-Shore Transports

[38] Supported by two complementary data sets, we showed consistently that the alongshore wind stress is upwelling-favorable almost all year long at various locations along the coast (Figure 3). Strong to moderate theoretical offshore Ekman transport is obtained between 21.5° and 26.5°S all year round, although intensified for the austral spring and summer. From 26.5° to 31°S, the alongshore wind stress is strongly upwelling favorable during the spring and summer months and remains weak during late autumn and winter. South of 31°S, the theoretical Ekman transport is offshore from late spring to the end of the summer, maximized at 34°S, in very good agreement with *Gersbach et al*. [1999], while it shows neutral to reverse downwelling conditions during autumn/winter months. The general wind patterns are also in good agreement with the wind roses computed from land-based measurements by *Pattiaratchi and Woo* [2009].

[39] Conversely to *Smith et al*. [1991]'s suggestion of a constant alongshore geopotential gradient responsible for driving the LC, we found that it shows important spatiotemporal variations (Figure 4), in accord with *Godfrey and Ridgway* [1985]. However, the important variability of the geostrophic limitation suggests a strong influence of mesoscale structures such as eddies and meanders of the LC, in good agreement with the geostrophic inflow estimates of *Weller et al*. [2011]. Based on both in situ and modeled data, they showed that mesoscale variability generated distinct zones of enhanced onshore/offshore transport along the shelf break. The latter statement is supported by the observational study of *Lowe et al*. [2012] which evokes that the alongshore geopotential gradient is not constant throughout the year since there is no consistent phasing between the poleward flow and the alongshore wind stress. It also suggests that the circulation may sometimes be

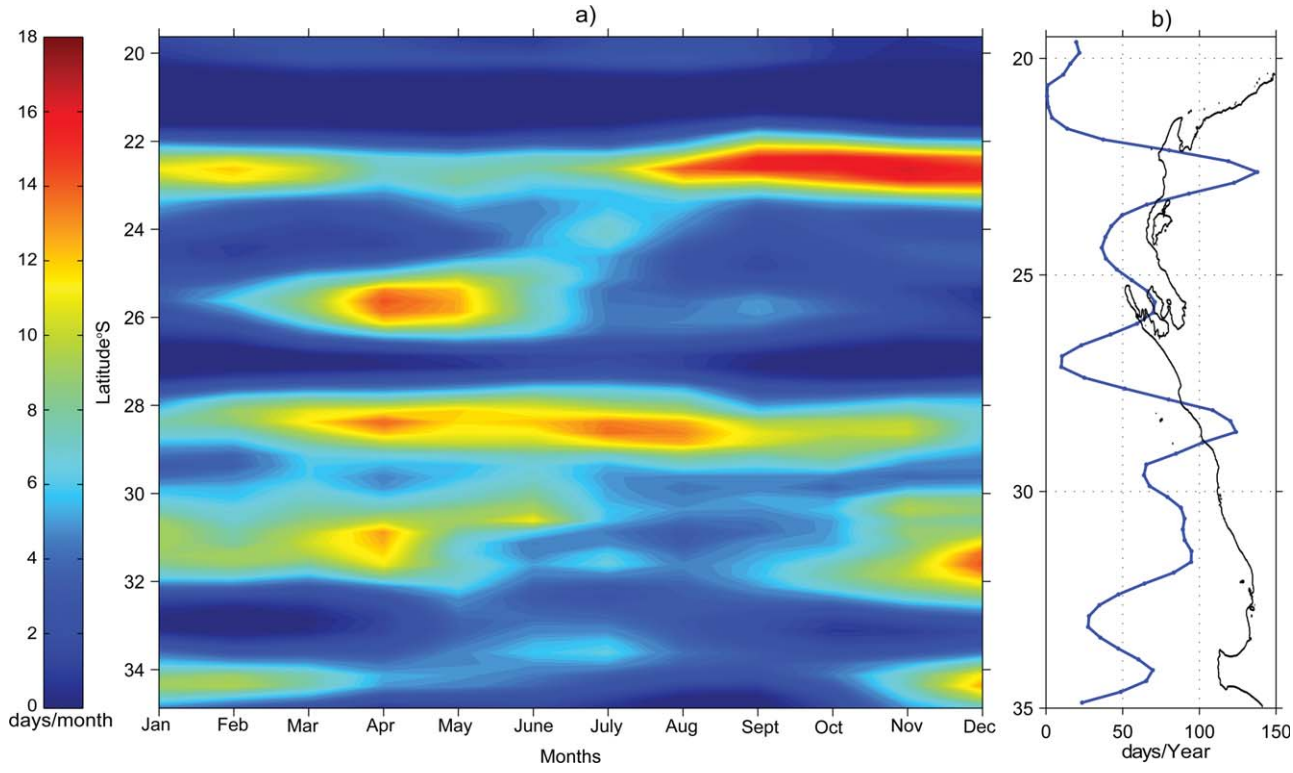

Figure 7. Climatological analysis of sporadic upwelling events. (a) Hovmöller (latitude versus time) diagram of the mean number of "upwelling days" (CUI > 15 m/day during 3 days or more) per month and (b) mean number of "upwelling days" per year, recorded over the period 1995–2010.

strongly influenced by eddies, current meandering, and other mesoscale features that complicate the cross-shore flow. Whether the seasonal variations of the LC intensity are modulated by the variations in the magnitude of the opposing seasonal wind stress, by the alongshore pressure gradient itself, or by a combination of both, is still subject to debate.

[40] Alternating geostrophic flows were indeed found at around 25–27°S, possibly related to the sharp change in the orientation of the coastline (see Figure 1), creating an offshoot of the LC and favoring meandering and mesoscale eddy formation [*Rennie et al*., 2007]. *Marchesiello and Estrade* [2010] also found that offshore flows usually occur downstream of the major promontories in eastern-boundary upwellings. Another hypothesis would be the influence of the Shark Bay outflow potentially driving density currents originating from the inner shelf [*Pattiaratchi et al*., 2011]. South of 28°S, we also observed transient weak onshore geostrophic flow that can be associated with permanent eddy-like features forming around the Abrolhos archipelago, [*Rennie et al*., 2007; *Meuleners et al*., 2007].

[41] Seasonal variations in the source waters of the LC could also help explain the variability of the geostrophic inflow. It is well known that the LC accelerates down the west coast of Australia, with at least some of its water sourced from onshore geostrophic flow between 23° and 30°S [*Domingues et al*., 2007; *Meuleners et al*., 2007]. *Smith et al*. [1991] speculated that there may also be some seasonal variations in these source waters, with more onshore entrainment of subtropical waters south of 23°S during late winter and conversely a more tropical water source from the North West Shelf during autumn. This is consistent with the measurements of *Lowe et al*. [2012], which showed that the LC peaks in autumn at 22°S, somehow earlier than further south. Our results also revealed a stronger onshore geostrophic limitation in April-June north of 25°S, whereas it is translated later in June-August south of 30°S (see Figure 5b). *Domingues et al*. [2007] and *Meuleners et al*. [2007] speculated that the late intensification of the LC south of 28°S is caused by onshore flow in late winter providing additional sources to the LC, leading to change in its temperature and salinity signature by entrainment of cooler, more saline oceanic subtropical waters [*Weller et al*., 2011].

4.3. Factors Influencing the Ekman/Geostrophy Balance

[42] Overall, the CUI is positive during spring/summer, as a combined effect of the strong alongshore wind stress during the austral spring/summer associated with a thinner MLD, and weak or negative during autumn/winter months (Figure 5). Indeed, when resolving EUI + GUI = 0 (following equation (1)) as a function of D for a given alongshore wind stress τ_a, we find that:

$$U_G = 2\tau_a/(\rho f D) \tag{5}$$

[43] U_G being inversely proportional to D, it indicates that for thicker $D \approx$ MLDs, a weaker onshore geostrophic limitation is needed to counteract the favorable wind forcing. However, the MLD effect is more puzzling since it also affects the source of the upwelled water. Indeed, *Lowe*

et al. [2012] suggested that the deeper MLD in autumn/winter is transferring the onshore Ekman return flow deeper below the MLD, favoring deeper origins of the upwelled waters against a shallower source during the periods of strong summer stratification. This is also consistent with the observations of *Rossi et al*. [2013] who estimate the origin of upwelled waters up to 150 m in autumn, whereas it was documented at only 100 m in the austral summer [*Hanson et al*., 2005].

[44] Another general observation is the higher CUI in the northern coastal areas of West Australia as compared to the southern ones. This can be related to the effect of a stronger wind stress in the lower latitudes overcoming the negative influence of a thicker MLD. In addition, higher latitude upwelling should be more affected by the geostrophic limitation. With $D = \pi\sqrt{2A_V/|f|}$, equation (5) can be rewritten as

$$U_G = 2\tau_a/\left(\pi\rho\sqrt{2A_V|f|}\right) \quad (6)$$

which indicates that for a given wind stress τ_a, the opposing geostrophic current required to compensate the Ekman transport is larger at lower latitudes than at higher ones [*Marchesiello and Estrade*, 2010].

[45] Looking at equation (1), an extended shelf width (large L_U) will enhance the geostrophic onshore velocities and dampen the offshore Ekman transport equally. It is, however, necessary to include the continental shelf structure in the model to account for the difference between the intense upwelling observed over narrow continental shelves (such as in the Humboldt system) and the weaker upwelling observed over large and shallow shelves (such as in southern Morocco, as discussed by *Marchesiello and Estrade* [2010]). Note there is also the indirect effect of a wider shelf on the mean position of the LC. Since the LC core is more or less aligned with the shelf break [*Pattiaratchi and Woo*, 2009], its mean position and associated onshore geostrophic limitation will be concentrated further from the coast, thus providing a wider innershelf region for the Ekman divergence to take place.

[46] The sensitivity of CUI to different values of parameters A_V and A_H has been tested and the analysis (not shown) revealed that L_U (and thus CUI) is almost insensitive to small changes in the horizontal viscosity A_H. However, CUI is significantly affected by the choices of A_V. In particular, a larger vertical viscosity results in deeper $D \approx$ MLD and larger L_U, which thus leads to a negative effect on upwelling development. Conversely, a lower vertical viscosity results in shallower $D \approx$ MLD and smaller L_U, thus enhancing the upwelling development.

4.4. Occurrence of Sporadic Upwelling Over the West-Australian Coast

[47] We have shown that contrary to prior belief sporadic upwelling along the WA coast is favored not only in summer months, but also roughly from mid-August to mid-April (Figure 7), extending the conclusions of *Lowe et al*. [2012] at the Ningaloo Peninsula. About 90% of the recorded events last between 3 and 10 days, thus coinciding with the dominant timescale of wind forcing, within the synoptic band of weather patterns (1–2 weeks) in the Western Australia region [*Cresswell et al*., 1989; *Pattiaratchi and Woo*, 2009]. The transient upwelling events are indeed periodically established because of the variations in the equatorward winds on a weekly timescale.

[48] Due to a combination of factors already mentioned (strong alongshore wind stress, limited onshore geostrophic flow and narrow continental shelves mainly), the latitudes 22.5°, 28.5°, 31.5°, and 34°S benefit preferentially from an upwelling favorable balance. Sporadic upwelling events have been previously documented off the Ningaloo peninsula [*Hanson et al*., 2005; *Woo et al*., 2006; *Lowe et al*., 2012], in the Geelvink Channel [*Cresswell et al*., 1989; *Pattiaratchi and Woo*, 2009], and in the southwest region [*Pearce and Pattiaratchi*, 1999; *Gersbach et al*., 1999] but not yet over the narrow shelf north of Perth (31.5°S).

[49] When counting individual events, there are between 8 and 18 upwelling favorable days per month during spring/summer, whereas it is between 0 and 5 days in autumn/winter, except at specifically favored areas. Comparing two of these locations along the WA coast, there are between 8 and 10 days favorable for upwelling per month at 34°S almost exclusively during summer (November–April), whereas it is between 0 and 3 days for the rest of the year. At 22.5°S, both the timing and the amplitude of the events are different with upwelling favorable conditions almost all year long, characterized by 11–18 days in the upwelling season (September–March) and 6–8 days from May to July. Moreover, we found that in the Ningaloo region (22.5°S), the upwelling events are significantly longer than anywhere on the coast, with about 20% of the events lasting more than 15 days. Therefore, the steep continental shelf offshore of the Ningaloo Peninsula, combined with the strong near-persistent alongshore wind and low geostrophic limitation appear to maximize the occurrence and the duration of upwelling events there.

4.5. General Discussion

[50] These transient upwelling events are in general not able to directly feed the offshore waters through filament formation and Ekman drift as in other typical eastern-boundary currents because of the presence of the LC. Hence, productive upwelled waters are likely to be confined inshore and advected northward in the coastal countercurrent systems [e.g., *Rossi et al*., 2013], possibly compensating for the localized character of these events. This might have important implications for the coastal oceanography of shelf and lagoon ecosystems as suggested by *Wyatt et al*. [2012] who showed a strong link between the activity of the fringing coral reef at Ningaloo (21.5–23°S) and the surrounding oceanographic conditions. We hypothesize that Ningaloo reef and its associated fauna and flora benefit from enriched waters all year long because (i) during spring/summer, numerous sporadic upwelling events happen locally and are associated with moderate nutrient enrichment (shallow MLD) and (ii) during winter/autumn, transient upwelling events still occur locally, while the northward advection of upwelled waters further south adds a contribution, all being characterized by elevated nutrient concentration (deep MLD and shallow low dissolved oxygen/high nitrate (LDOHN) layer) [*Rossi et al*., 2013]. These complex biophysical processes impacting the coastal productivity of the world heritage listed Ningaloo peninsula

provide new mechanisms to meet the nutritional requirement from both shallow benthic communities of the reef [*Wyatt et al*., 2012] and their associated pelagic mega fauna [*Taylor and Pearce*, 1999].

[51] Finally, *Moore et al*. [2007] observed that only anticyclonic eddies carry elevated levels of inorganic nutrients and biomass in the LC system. *Dietze et al*. [2009] suggested that this is due to the injection of enriched shelf waters starting with the formation of eddies in April–May. It coincides with the presence of a shallow source of nutrients [*Rossi et al*., 2013] and with the occurrence of sporadic upwelling events. We speculate that anticyclonic eddies, forming at preferential periods/locations, could match sporadic upwelling events in space and time and thus entrain shelf enriched waters offshore. This associative mechanism might extend the influence of the coastal sporadic upwelling events several hundred kilometers offshore.

5. Conclusions

[52] While the LC does not allow persistent upwelling along the Western Australian coastline, sporadic upwelling events were documented. In this work, we investigated their occurrence along the entire coast over the seasonal cycle using high-resolution remotely sensed data. Transient events lasting 3–10 days are likely to occur preferentially from September to April at specific latitudes, with 8–10 upwelling days per month at 31.5°S and 34°S and up to 18 days per month at 22.5°S for a longer period. Although generally favored during the spring/summer season, we have shown that sporadic upwelling events do happen all year long north of 30°S. At these locations (22.5°, 25.5°, and 28.5°S), the sparse winter/autumn events (2–8 upwelling days per month) are likely to provide higher nutrient inputs due to a deeper source beneath the MLD. However, it takes stronger wind forcing to uplift the deep nutrients in winter. Overall, the Ningaloo region (22.5°S) cumulates the highest total number of upwelling days over 15 year period and is characterized by longer events.

[53] This high variability is mainly due to a combination of: Near-consistent favorable wind stress in lower latitudes, important variations of the geostrophic limitation, seasonal changes of the MLD, and local topographic factors. To explain the variability of the geostrophic limitation, several hypotheses have been discussed such as a modification of the LC through subtropical geostrophic injection and the flow instabilities associated with meandering and mesoscale eddy formation.

[54] Overall, the biological impact of localized upwelling over the WA coast is a function of (a) the strength and duration of upwelling-favorable winds, (b) the intensity of the onshore limitation (driven by the LC and its associated mesoscale structures), (c) the physical characteristics within the LC (e.g., MLD and nitracline, itself influenced by the presence of the LDOHN), and (d) the local topography. It suggests that nutrient enrichment might occur at any time of the year at many locations on the WA coast while being relatively short lived (∼10 days) and of variable magnitude.

[55] **Acknowledgments.** This research was supported under Australian Research Council's Discovery Project funding scheme (DP1093510) which also supports V.R. acknowledges support from MICINN and FEDER through project ESCOLA (CTM2012-39025-C02-01) while revising this paper. M.F. is supported by the CSIRO Wealth from Oceans Flagship. The authors acknowledge J. Sudre who provided the satellite archives. QuikSCAT and SeaWinds data are produced by Remote Sensing Systems and sponsored by the NASA Ocean Vector Winds Science Team. The authors would like to thank the anonymous reviewers for their valuable comments that have substantially improved this manuscript.

References

Antonov, J. I., D. Seidov, T. P. Boyer, R. A. Locarnini, A. V. Mishonov, H. E. Garcia, O. K. Baranova, M. M. Zweng, and D. R. Johnson (2010), World Ocean Atlas 2009, vol. *2*, Salinity, edited by S. Levitus, 184 pp., *NOAA Atlas NESDIS 69*, U.S. Gov. Print. Off., Wash., D. C.

Alvarez, I., M. Gomez-Gesteira, M. deCastro, and J. M. Dias (2008), Spatio-temporal evolution of upwelling regime along the western coast of the Iberian Peninsula, *J. Geophys. Res.*, *113*, C07020, doi:10.1029/2008JC004744.

Bakun, A. (1990), Global climate change and intensification of coastal upwelling, *Science*, *247*, 198–201, doi:10.1126/science.247.4939.198.

Cresswell, G. R., and T. J. Golding (1980), Observations of a south flowing current in the southeastern Indian Ocean, *Deep Sea Res. Part A*, *27*, 449–466.

Cresswell, G. R., F. M. Boland, J. L. Peterson, and G. S. Wells (1989), Continental shelf currents near the Abrolhos Islands, Western Australia, *Aust. J. Mar. Freshwater Res.*, *40*, 113–128.

Condie, S. A., and J. R. Dunn (2006), Seasonal characteristics of the surface mixed layer in the Australasian region: Implications for primary production regimes and biogeography, *Mar. Freshwater Res.*, *57*, 569–550.

Dietze, H., R. Matear, and T. Moore (2009), Nutrient supply to anticyclonic meso-scale eddies off Western Australia estimated with artificial tracers released in a circulation model, *Deep Sea Res. Part I*, *56*, 1440–1448.

Domingues, C. M., M. E. Maltrud, S. E. Wijffels, J. A. Church, and M. Tomczak (2007), Simulated Lagrangian pathways between the Leeuwin Current System and the upper-ocean circulation of the southeast Indian Ocean, *Deep Sea Res. Part II*, *54*(8–10), 797–817.

Feng, M., G. Meyers, A. F. Pearce, and S. Wijffels (2003), Annual and interannual variations of the Leeuwin Current at 32°S, *J. Geophys. Res.*, *108*, 3355, doi:10.1029/2002JC001763.

Feng, M., A. Biastoch, C. Boning, N. Caputi, and G. Meyers (2008), Seasonal and interannual variations of upper ocean heat balance off the west coast of Australia, *J. Geophys. Res.*, *113*, C12025, doi:10.1029/2008JC004908.

Feng, M., M. J. McPhaden, S.-P. Xie, and J. Hafner (2013), La Niña forces unprecedented Leeuwin Current warming in 2011, *Nat. Sci. Rep.*, *3*, 1277, doi:10.1038/srep01277.

Furnas, M. (2007), Intra-seasonal and inter-annual variations in phytoplankton biomass, primary production and bacterial production at North West Cape, Western Australia: Links to the 1997–1998 El Niño event, *Cont. Shelf Res.*, *27*, 958–980.

Gersbach, G. H., C. B. Pattiaratchi, G. N. Ivey, and G. R. Cresswell (1999), Upwelling on the south-west coast of Australia—Source of the Capes current?, *Cont. Shelf Res.*, *19*, 363–400.

Godfrey, J. S., and K. R. Ridgway (1985), The large-scale environment of the poleward-flowing Leeuwin Current, Western Australia: Longshore steric height gradients, wind stresses and geostrophic flow, *J. Phys. Oceanogr.*, *15*(5), 481–495.

Hanson, C. E., and A. D. McKinnon (2009), Pelagic ecology of the Ningaloo region, Western Australia: Influence of the Leeuwin Current, *J. R. Soc. West. Aust.*, *92*, 129–137.

Hanson, C. E., C. B. Pattiaratchi, and A. M. Waite (2005), Sporadic upwelling on a downwelling coast: Phytoplankton responses to spatially variable nutrient dynamics off the Gascoyne region of Western Australia, *Cont. Shelf Res.*, *25*, 1561–1582.

Locarnini, R. A., A. V. Mishonov, J. I. Antonov, T. P. Boyer, H. E. Garcia, O. K. Baranova, M. M. Zweng, and D. R. Johnson, (2010), *World Ocean Atlas 2009*, vol. *1*, Temperature, edited by S. Levitus, 184 pp., NOAA Atlas NESDIS 68, U.S. Gov. Print. Off., Wash., D. C.

Lourey, M. J., J. R. Dunn, and J. Waring (2006), A mixed-layer nutrient climatology of Leeuwin Current and Western Australian shelf waters: Seasonal nutrient dynamics and biomass, *J. Mar. Syst.*, *59*, 25–51.

Lowe, R. J., G. N. Ivey, R. M. Brinkman, and N. L. Jones (2012), Seasonal circulation and temperature variability near the North West Cape of Australia, *J. Geophys. Res.*, *117*, C04010, doi:10.1029/2011JC007653.

Marchesiello, P., and P. Estrade (2010), Upwelling limitation by onshore geostrophic flow, *J. Mar. Res.*, *68*, 37–62.

Meuleners, M. J., C. B. Pattiaratchi, and G. N. Ivey (2007), Numerical modelling of the mean flow characteristics of the Leeuwin current system, *Deep Sea Res. Part II*, *54*, 837–858.

Moore, T. S., S. Thomas, R. J. Matear, J. Marra, and L. Clementson (2007), Phytoplankton variability off the Western Australian Coast: Mesoscale eddies and their role in cross-shelf exchange, *Deep Sea Res. Part II*, *54*, 943–960.

Nykjaer, L., and L. Van Camp (1994), Seasonal and interannual variability of coastal upwelling along northwest Africa and Portugal from 1981 to 1991, *J. Geophys. Res.*, *99*, 14,197–14,208.

Pattiaratchi, C., and M. Woo (2009), The mean state of the Leeuwin Current system between North West Cape and Cape Leeuwin, *J. R. Soc. West. Aust.*, *92*, 221–241.

Pattiaratchi, C., B. Hollings, M. Woo, and T. Welhena (2011), Dense shelf water formation along the south-west Australian inner shelf, *Geophys. Res. Lett.*, *38*, L10609, doi:10.1029/2011GL046816.

Pauly, D., and V. Christensen (1995), Primary production required to sustain global fisheries, *Nature*, *374*, 255–257.

Pearce, A., and C. Pattiaratchi (1999), The Capes Current: A summer countercurrent flowing past Cape Leeuwin and Cape Naturaliste, Western Australia, *Cont. Shelf Res.*, *19*(3), 401–420.

Pickett, M. H., W. Tang, L. K. Rosenfeld, and C. H. Wash (2003), QuikSCAT satellite comparison with nearshore buoy wind data off the U.S. west coast, *J. Atmos. Oceanic Technol.*, *20*, 1869–1879.

Rennie, S. J., C. Pattiaratchi, and R. D. McCauley (2007), Eddy formation through the interaction between the Leeuwin Current, Leeuwin Undercurrent and topography, *Deep Sea Res. Part II*, *54*, 818–836.

Ridgway, K. R., and S. A. Condie (2004), The 5500-km-long boundary flow off western and southern Australia, *J. Geophys. Res.*, *109*, C04017, doi:10.1029/2003JC001921.

Rio, M.-H., P. Schaeffer, G. Moreaux, J.-M. Lemoine, and E. Bronner (2009), *A new mean dynamic topography computed over the global ocean from GRACE data, altimetry and in-situ measurements, paper presented at OceanObs'09 Symposium*, Venice, Italy, IOC/UNESCO and ESA.

Rossi, V., M. Feng, C. Pattiaratchi, M. Roughan, and A. M. Waite (2013), Linking synoptic forcing and local mesoscale processes with biological dynamics off Ningaloo Reef, *J. Geophys. Res. Oceans*, *118*, doi:10.1002/jgrc.20110.

Rousseaux, C. S. G., R. Lowe, M. Feng, A. M. Waite, and P. A. Thompson (2012), The role of the Leeuwin Current and mixed layer depth on the autumn phytoplankton bloom off Ningaloo Reef, Western Australia, *Cont. Shelf Res.*, *32*, 22–35.

Smith, R. L., A. Huyer, J. S. Godfrey, and J. A. Church (1991), The Leeuwin current off Western Australia, 1986–1987, *J. Phys. Oceanogr.*, *21*, 323–345.

Sudre, J., C. Maes, and V. Garçon (2013), On the global estimates of geostrophic and Ekman surface currents, *Limnol. Oceanogr. Fluids Environ.*, *3*, 1–20.

Taylor, J. G., and A. F. Pearce, (1999), Ningaloo Reef currents: Implications for coral spawn dispersal, zooplankton and whale shark abundance, *J. R. Soc. West. Aust.*, *82*, 57–65.

Thompson, R. O. R. Y. (1987), Continental shelf—Scale model of the Leeuwin current, *J. Mar. Res.*, *45*, 813–827.

Weaver, A. J., and J. H. Middleton (1989), On the dynamics of the Leeuwin current, *J. Phys. Oceanogr.*, *19*, 626–648.

Weller, E., D. Holliday, M. Feng, L. Beckley, and P. A. Thompson (2011), A continental shelf scale examination of the Leeuwin Current off Western Australia during the austral autumn-winter, *Cont. Shelf Res.*, *31*, 1858–1868.

Woo, M., and C. B. Pattiaratchi (2008), Hydrography and waters masses off the Western Australian coast, *Deep Sea Res. Part I*, *55*, 1090–1104.

Woo, M., C. B. Pattiaratchi, and W. Schroeder (2006), Summer surface circulation along the Gascoyne continental shelf, Western Australia, *Cont. Shelf Res.*, *26*, 132–152.

Wyatt, A. S. J., J. L. Falter, R. J. Lowe, S. Humphries, and A. M. Waite (2012), Oceanographic forcing of nutrient uptake and release over a fringing coral reef, *Limnol. Oceanogr.*, *57*(2), 401–419.

Zhang, H.-M., J. J. Bates, and R. W. Reynolds (2006), Assessment of composite global sampling: Sea surface wind speed, *Geophys. Res. Lett.*, *33*, L17714, doi:10.1029/2006GL027086.